JTTEE5 18:209–216
DOI: 10.1007/s11666-009-9311-8
1059-9630/$19.00 © ASM International

The Effect of Heat Treatment on the Oxidation Behavior of HVOF and VPS CoNiCrAlY Coatings

S. Saeidi, K.T. Voisey, and D.G. McCartney

(Submitted October 16, 2008; in revised form February 26, 2009)

Free-standing VPS and HVOF CoNiCrAlY coatings were produced. The as-sprayed HVOF coating retained the γ/β microstructure of the feedstock powder, and the VPS coating consisted of a single (γ) phase. A 3-h, 1100 °C heat treatment in vacuum converted the single-phase VPS coating to a two-phase γ/β microstructure and coarsened the γ/β microstructure of the HVOF coating. Oxidation of free-standing as-sprayed and heat-treated coatings of each type was carried out in air at 1100 °C for a duration of 100 h. Parabolic rate constant(s), K_p, were determined for free-standing, as-sprayed VPS and HVOF coatings as well as for free-standing coatings that were heat treated prior to oxidation. The observed increase in K_p following heat treatment is attributed to a sintering effect eliminating porosity from the coating during heat treatment. The lower K_p values determined for both HVOF coatings compared to the VPS coatings is attributed to the presence of oxides in the HVOF coatings, which act as the barrier to diffusion. Oxidation of the as-sprayed coatings produced a dual-layer oxide consisting of an inner α-Al_2O_3 layer and outer spinel layer. Oxidation of the heat-treated samples resulted in a single-layer oxide, α-Al_2O_3. The formation of a thin α-Al_2O_3 layer during heat treatment appeared to prevent nucleation and growth of spinel oxides during subsequent oxidation.

Keywords CoNiCrAlY, heat treatment, HVOF, oxidation, thermally grown oxide, VPS

1. Introduction

MCrAlY (M = Ni, Co, or both) coatings are commonly used as overlay coatings and as bond coats for thermal barrier coatings (TBCs) composed of yttria-stabilized zirconia (YSZ) in order to protect turbines from high-temperature oxidation (Ref 1-4). These coatings owe their protective effect to the fact that aluminum forms a continuous oxide layer on the coating surface that is thermally very stable while the remaining elements (e.g., Cr) control the aluminum activity, hold the oxide in place (e.g., Y) and adapt the coating to the properties of the base material (Ref 5, 6). Premature failure of TBCs during thermal cycling is still a critical problem, which limits the lifetime of the coated components (Ref 7). This failure mainly occurs by delamination of the top coat (Ref 8, 9). The cracks leading to delamination nucleate and propagate at the top-bond coat interface. Interfacial oxides, in particular, the thermally grown oxide (TGO) layer, play an important role in the cracking process (Ref 4).

S. Saeidi, K.T. Voisey, and **D.G. McCartney**, Department of Mechanical, Materials and Manufacturing Engineering, Faculty of Engineering, University of Nottingham, Nottingham, UK. Contact e-mails: emxss1@nottingham.ac.uk, sam_saidi2001@yahoo.com, katy.voisey@nottingham.ac.uk, and graham.mccartney@nottingham.ac.uk.

As the oxidation behavior of the thermally sprayed MCrAlY is significantly influenced by the coating process and the composition of the alloy (Ref 3), and plays a major role in the TBC failure, the results of a study into the oxidation behavior of free-standing High Velocity Oxy-Fuel (HVOF) and Vacuum Plasma Sprayed (VPS) CoNiCrAlY coatings are presented in this study. The oxidation of as-sprayed and heat-treated samples was carried out at 1100 °C for a duration of 100 h and their microstructural features were characterized by x-ray diffraction (XRD) and scanning electron microscopy (SEM) equipped with energy dispersive spectroscopy (EDS).

1.1 Experimental Methods

A CoNiCrAlY powder supplied by Praxair (CO-210-24) was used for both VPS and HVOF spraying. Powder size was (45 ± 20 μm), with a mean particle diameter, D(v, 0.5), of 34 μm, and its nominal composition is given in Table 1. The as-received powder had a two-phase microstructure. The XRD and EDS results identified the presence of γ and β phases; the γ phase is fcc and is Co rich with a lattice parameter of 0.358 nm, the β phase is (Co, Ni)Al, an ordered B2, bcc, structure with a lattice parameter of 0.286 nm (Ref 10, 11).

Mild steel substrates were used for both forms of spraying: 60 × 25 × 1.8 mm substrates were used for HVOF, whereas slightly smaller, 60 × 20 × 1.8 mm, substrates were used for VPS. Prior to spraying, the substrates were ground with 800 grade SiC paper, rather than being grit blasted, in order to enable coating detachment after spraying.

HVOF spraying was carried out using a commercial MetJet II (Metallization) gun. Kerosene was used as fuel and nitrogen as the carrier gas. Compressed air jets were used to cool the samples during and after spraying. The substrates were mounted on a rotating sample holder while the spray gun traversed vertically.

For the VPS spraying, a Plasma TECHNIK VPS system was used. The VPS chamber was first evacuated and back filled with Ar and waiting times of 20 seconds per pass were allowed. The spraying parameters employed for each spraying system are given in Table 2.

Table 1 Chemical composition of the powder, wt.%

Co	Ni	Cr	Al	Y
38.5	32	21	8	0.5

Table 2 Spraying parameters

HVOF		VPS	
Spray distance, mm	356	Spray distance, mm	280
Substrate cooling	Air	Current, A	600
Traverse speed, m/s	1	Voltage, V	63
N_2 carrier gas flow rate, L/min	5.5	Power, kW	40
O_2 gas flow rate, L/min	890	Air flow, L/min	50
Kerosene flow rate, mL/min	470	H_2 flow, L/min	10
Nozzle length, mm	100	Traverse speed, mm/s	84

After the spraying process, both HVOF and VPS coatings were detached from their substrates by bending the substrate. Because of the deposition of large coating thickness (~600 μm) and the fact that the substrates were ground to an 800 grit finish prior to spraying, bending the substrate was sufficient to detach the coating.

The heat treatment of free-standing coatings was carried out at 1100 °C for 3 h in vacuum followed by furnace cooling, a typical heat treatment for coatings of this type (Ref 5, 10, 11). As-sprayed and heat-treated HVOF and VPS samples were then subjected to isothermal oxidation at 1100 °C in air for time periods of 1, 50, 75, and 100 h. After oxidation, specimens were removed from the furnace at temperature and cooled in laboratory air to room temperature.

Polished cross sections were characterized using a FEI XL30 scanning electron microscope equipped with energy dispersive spectroscopy (EDS). A Bruker x-ray diffractometer (XRD) with step size of 0.01° and 2-s counting time per step was used in order to analyze the presence of different phases. The relative proportions of each phase present in the coatings was determined using image analysis.

Continuous weight measurement of the as-sprayed and heat-treated samples during oxidation was also carried out using a thermogravimetric analyzer (TA Instruments SDT Q600). The reproducibility of the results was verified by running three shorter duration repeats for each sample type. By running the thermogravimetric analyzer without any samples present, it was confirmed that the initial peak

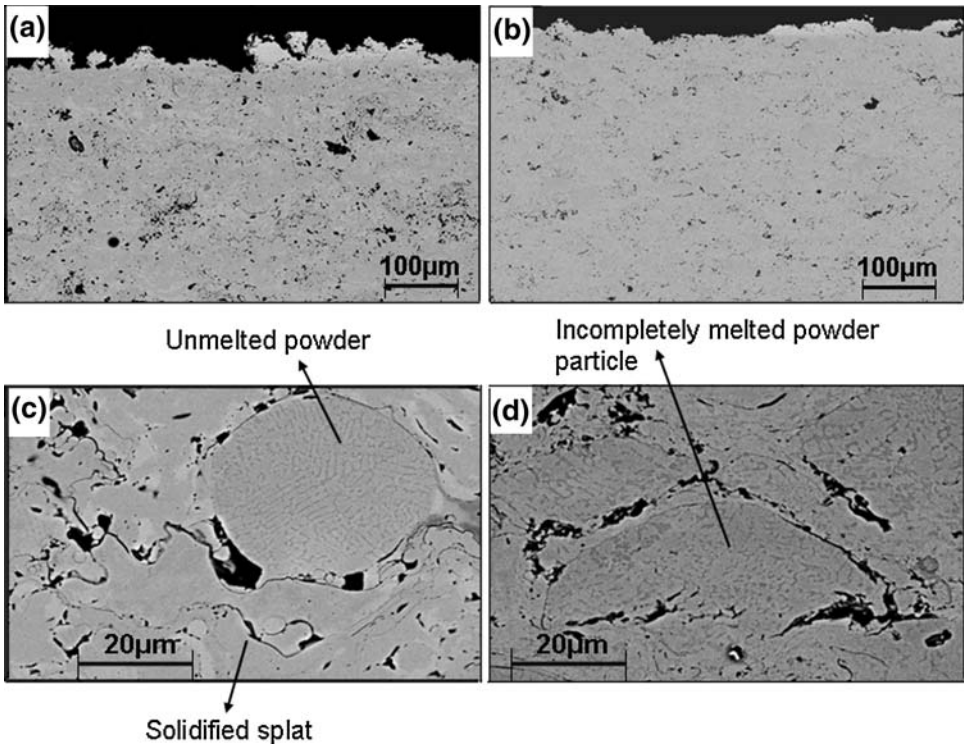

Fig. 1 SEM micrograph of cross section of (a) VPS coating, (b) HVOF coating, (c) VPS coating at higher magnification, (d) HVOF coating at higher magnification

seen in each set of results is a machine artifact. Parabolic rate constants were determined by plotting the square of the mass gain per unit area against time, and finding the gradient of the best straight-line fit to the results. This was carried out using the data from 500 min onward in order to omit the initial, artificial peak.

2. Results

2.1 Characterisation of Coatings

2.1.1 Characterisation of As-sprayed Coatings. Free-standing coatings of ~600 μm in thickness were obtained from both spraying methods. Examination of polished cross sections of the as-sprayed coatings showed that while there were only a few incompletely melted powder particles in the VPS coating, such particles were far more numerous in the HVOF coating (Fig. 1). The majority of the VPS coating was formed from well-flattened solidified splats (Fig. 1c).

As seen in the higher magnification SEM micrographs (Fig. 1c, d), the HVOF coating has retained the two-phase microstructure of the feedstock powder. The VPS coating mainly consists of a single phase, with a two-phase microstructure only retained in the unmelted powder particles. XRD (Fig. 2) clearly shows the presence of the γ phase in the VPS coating, the small amount of β present in the unmelted particles is insufficient to be detected, and therefore is estimated to be ≤2%. XRD confirmed the presence of both γ and β in the HVOF coating. The volume fractions of the phases present in each as-sprayed coating, as determined by image analysis, are given in Table 3.

2.1.2 Characterisation of Heat-Treated Coatings. Following the 3-h, 1100 °C vacuum heat treatment of the free-standing coatings, a two-phase structure was observed for both coatings. XRD confirmed this to be the same γ/β two-phase structure as previously seen in the feedstock powder and the as-sprayed HVOF coating. Comparison of Fig. 1(d) and 3(b) shows that heat treatment has resulted in coarsening of the β phase in the HVOF coating. The volume fractions of the phases present in each heat-treated coating, as determined by image analysis, are given in Table 3.

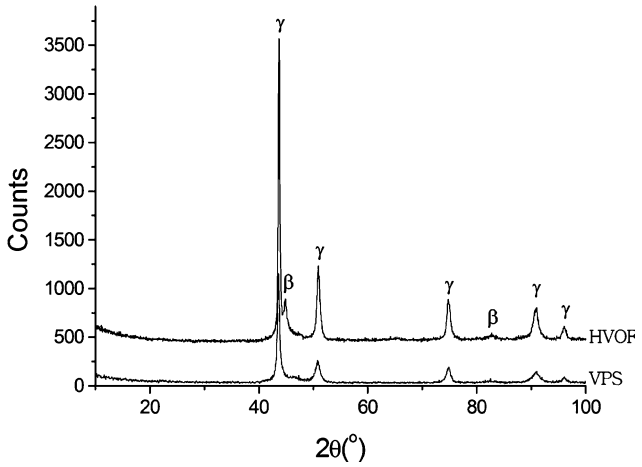

Fig. 2 XRD spectra for HVOF and VPS as-sprayed coatings

Table 3 Volume ratios of the phases present, as determined by image analysis

	HVOF		VPS	
	γ	β	γ	β
As-sprayed	~78	~22	~100	~0
Heat treated	~65	~35	~65	~35

2.2 Oxidation Results

2.2.1 Oxidation of As-Sprayed Coatings. Mass gain per unit area as a function of time for the as-sprayed coatings is shown in Fig. 4. The parabolic rate constants determined for the VPS and HVOF coatings are 5×10^{-10} and 3×10^{-10} $g^2\ cm^{-4}\ s^{-1}$, respectively.

The SEM micrographs in Fig. 5 show the oxide layers after various exposure times. An oxide layer is clearly visible for both coatings after 1 h. The oxide formed is a dual-layer oxide. EDS results show that the inner layer mainly consists of Al and O whereas the outer layer is a mixture of Co, Ni, Cr, and O. XRD spectra (Fig. 6) show the presence of α-Al_2O_3 and spinel oxides for both coatings. The inner oxide layer is therefore labeled as α-Al_2O_3 and the outer layer as a spinel oxide.

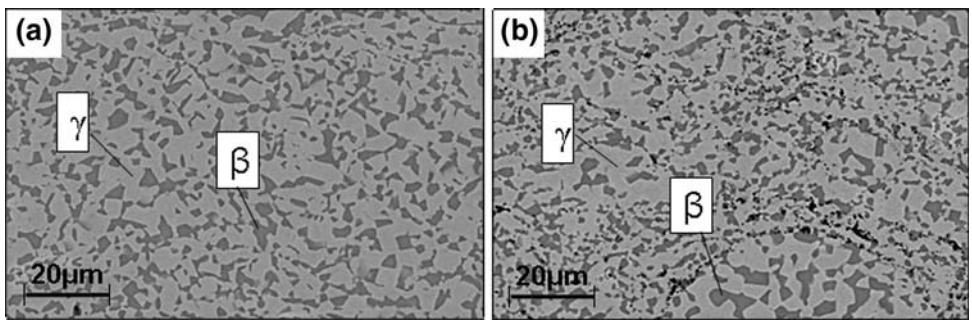

Fig. 3 SEM micrograph of (a) VPS, (b) HVOF heat-treated (3 h at 1100 °C) coatings

Spinel peaks in the XRD patterns were at slightly lower 2θ values than those expected for $NiAl_2O_4$ and $CoAl_2O_4$ and slightly higher than $NiCr_2O_4$ and $CoCr_2O_4$. EDS analysis showed that Co, Ni, Cr, Al, and O were all present in the outer oxide layer. Therefore, while the precise spinel present cannot be specified, we can say that it is either a mixture of some/all of the spinel-type oxides ($NiAl_2O_4$, $CoAl_2O_4$, $NiCr_2O_4$, $CoCr_2O_4$) or a substitutional solid solution $(Ni,Co)(Al,Cr)_2O_4$.

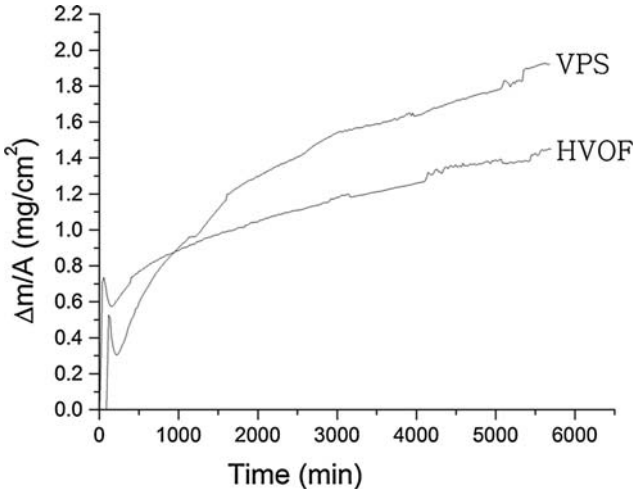

Fig. 4 Total weight change of as-sprayed HVOF and VPS coatings, at 1100 °C

As can be seen in Fig. 6 with increasing exposure time, the peaks related to the spinel-type oxides become higher in relative intensity suggesting a higher spinel oxide thickness, and this is confirmed by the SEM images in Fig. 5. Mixed oxide protrusions were observed for both coatings; however, these were more pronounced for the VPS coating as is shown in the 100-h micrograph in Fig. 5. Isolated brighter regions are seen within these protrusions. EDS results are consistent with these areas being NiO, as previously reported by other authors (Ref 12).

2.2.2 Oxidation of Heat-Treated Coatings. Mass gain as a function of time for the heat-treated coatings is shown in Fig. 7. The parabolic rate constants determined for the VPS and HVOF coatings are 1×10^{-9} and 4×10^{-10} $g^2\ cm^{-4}\ s^{-1}$, respectively.

The development of the oxide layer with time is shown in Fig. 8. A single-layer oxide formed on both coatings. EDS and XRD (Fig. 9) results indicated that this layer is α-Al_2O_3. XRD also detected the presence of small amounts of other oxides including the spinel phases, $NiAl_2O_4$ and $NiCr_2O_4$. Both the XRD results and SEM images show that spinel oxides are present to a much lesser extent than that were seen for the as-sprayed coatings.

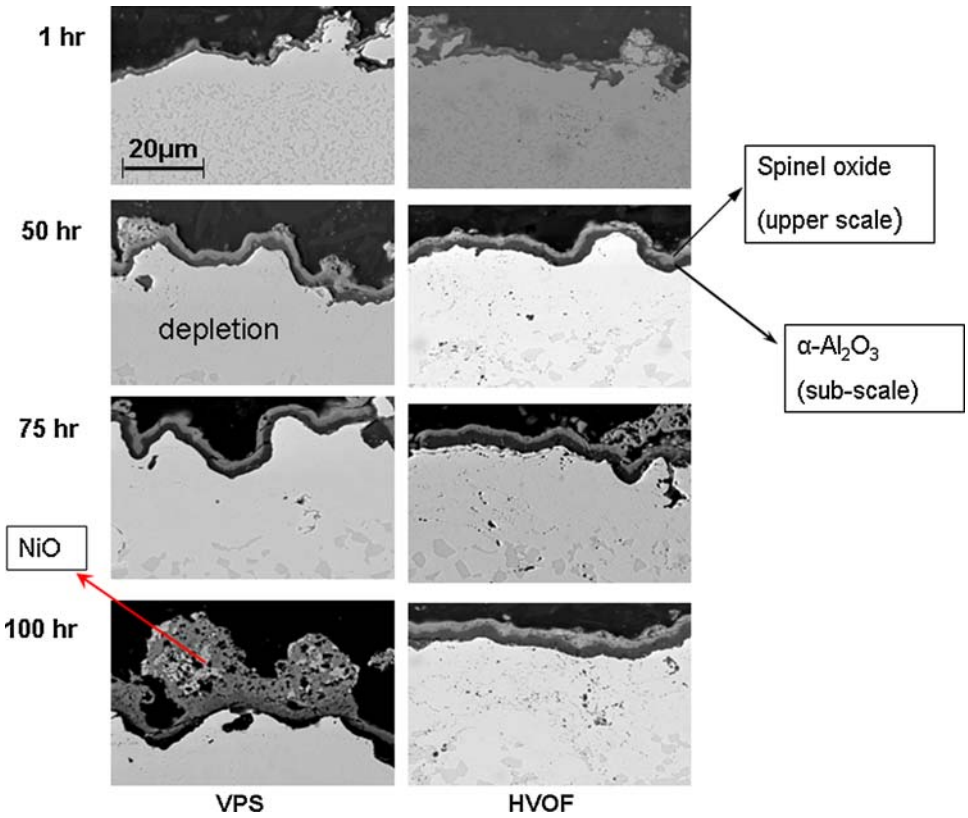

Fig. 5 Oxidation of VPS and HVOF coatings at 1100 °C for different exposure times, (all images are at the same magnification)

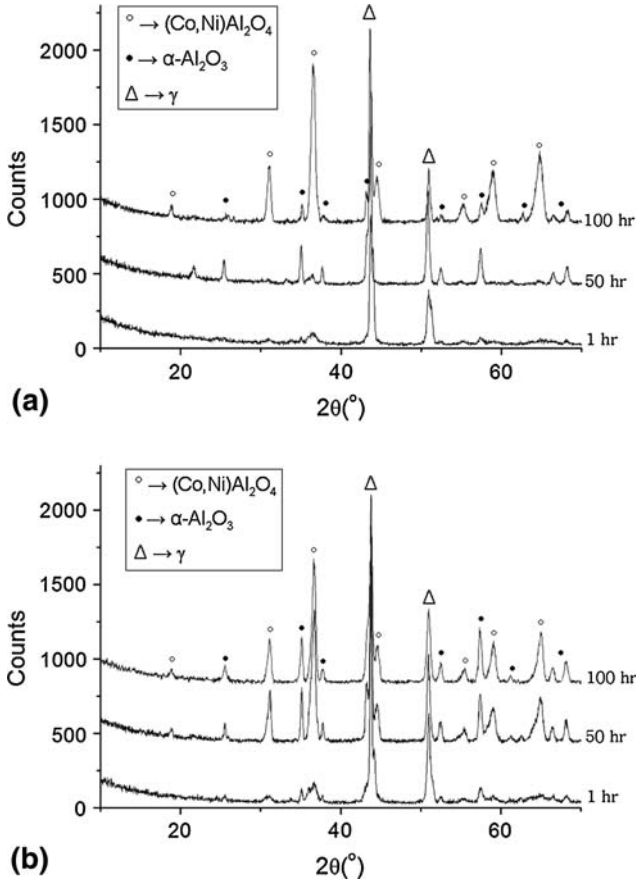

Fig. 6 XRD patterns from the as-sprayed oxidized surfaces for different oxidation times, (a) VPS, (b) HVOF

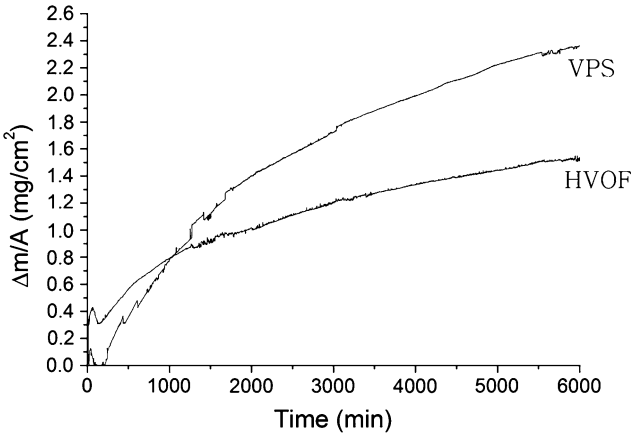

Fig. 7 Total weight change of heat-treated HVOF and VPS coatings, at 1100 °C

3. Discussion

The as-sprayed HVOF had a two-phase microstructure whereas the as-sprayed VPS coating had a largely single-phase structure. This difference results from the different temperatures experienced by the powder in each spraying process. In HVOF, the powder particles are exposed to a flame temperature of ~2700-3200 K for a relatively short time (Ref 13). This results in only partial melting of the powder. The dual phase γ/β microstructure of the feedstock powder is therefore retained in the resultant coating. In contrast, plasma spraying has a very high flame temperature >10000 K (Ref 13). Coupled with the lower particle velocity, this means that the powder is exposed to a higher temperature for a longer time. As a result, nearly all the powder particles melt during spraying and resolidify when being deposited on the substrate. The solidification is rapid, so that there is not enough time for the β-(Co,Ni)Al phase to precipitate out, resulting in the observed, single-phase, γ, microstructure.

The thermogravimetric analyzer (TGA) results indicate that oxide growth on both as-sprayed and heat-treated VPS and HVOF coatings broadly follows the expected parabolic behavior. For both the as-sprayed and heat-treated coatings, the VPS coating has the larger parabolic rate constant, K_p. For each coating type, the effect of heat treatment prior to the TGA run is to increase K_p, with an increase of 100 and 33% seen for the VPS and HVOF coatings, respectively. The K_p values determined in this studyare in line with some previously published results (Ref 3).

Heat treatment converted the single phase, γ, as-sprayed VPS coating to the two-phase γ/β structure shared by both the as-sprayed and heat-treated HVOF coatings. If the observed change in K_p was linked to this change in structure, the heat treatment would be expected to make the behavior of the heat-treated coatings resemble each other more closely than the as-sprayed coatings. This is not observed—in fact the heat treatment increases the proportional difference in the K_p values of each coating type, and hence, changing the VPS coating to the two-phase structure is ruled out as an explanation for the difference in oxidation behavior seen after heat treatment.

Diffusion occurring during the heat treatment heals some of the porosity present in the as-sprayed coatings via a sintering effect, as can be seen if Fig. 1 and 3 are compared. The increase in K_p values seen for both coatings is attributed to this as the discontinuities caused by porosity will act as barriers to diffusion, the removal or decrease in porosity will therefore enhance diffusion within the coating. This results in an increased rate of supply of oxide-forming elements, in this case specifically Al, to the surface, and hence, an increased K_p. It is well established that in γ/β coatings of this type, the Al-rich β phase acts as an Al reservoir (Ref 14-16). As oxidation proceeds, Al diffuses from the β phase to the growing alumina layer, resulting in depletion of the β phase in the near surface regions. Hence, diffusion of Al through the coating is highly relevant to scale formation. The heat treatment has a greater effect on the VPS coating compared to the HVOF coating. This is attributed to the different extents of coating oxidation during HVOF and VPS spraying. Whilst no attempt has been made to directly compare

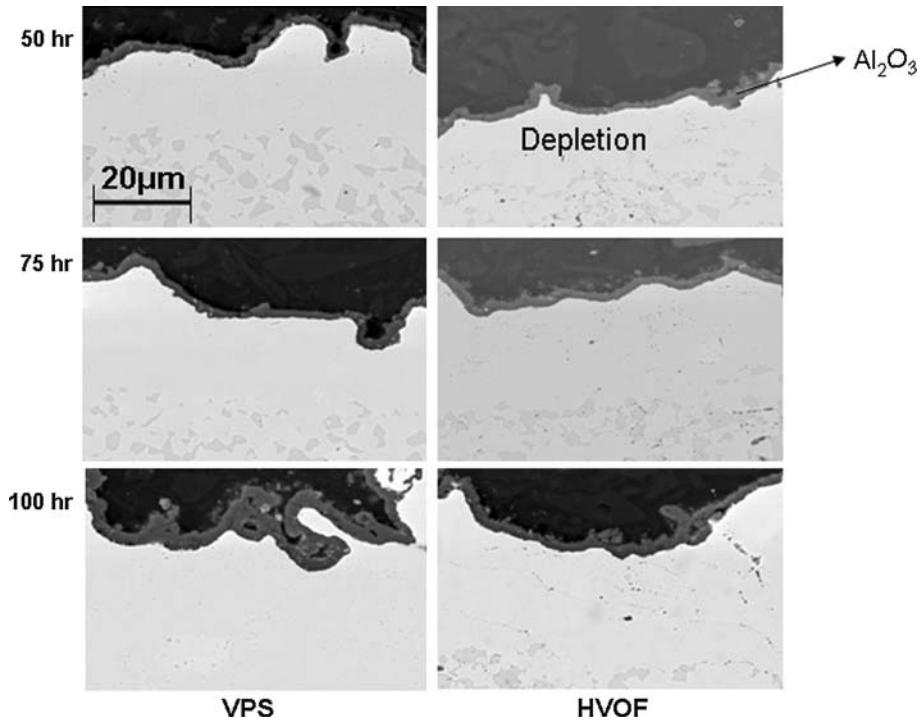

Fig. 8 SEM micrograph of heat-treated oxidized VPS and HVOF coatings at 1100 °C for different exposure times, (all the images have the same magnification)

oxide levels in this study, it is generally accepted that VPS coatings are essentially oxide free, because of being sprayed under vacuum. In HVOF coatings, on the other hand, a thin oxide layer is generated around each particle during spraying (Ref 17). It is suggested that these oxide layers are not affected by the heat treatment, and hence are retained in the heat-treated HVOF coating. They act as obstacles to diffusion, thereby inhibiting oxide growth. Hence, for HVOF coatings K_p is only slightly increased by heat treatment as only some obstacles to diffusion are removed. The idea that the oxides present in the HVOF coatings inhibit diffusion and hence result in a lower K_p also explains why the as-sprayed HVOF coating has a lower K_p than the oxide-free as-sprayed VPS coating. A similar effect and explanation has been previously put forward by Brandl et al. (Ref 18).

Oxidation of the as-sprayed coatings produced a dual layer oxide consisting of an inner layer of α-Al_2O_3 and an outer spinel layer. This dual-layer oxide is consistent with results previously reported by other researchers (Ref 19, 20). Oxidation of heat-treated samples resulted in the formation of a single layer, α-Al_2O_3, oxide. Of the two oxides considered, α-Al_2O_3 is the more thermodynamically stable, and hence will form at lower oxygen partial pressures. The kinetics of spinel oxide growth are greater than those of α-Al_2O_3. Therefore, if a clean MCrAlY surface is exposed to a sufficiently high oxygen partial pressure, both spinel oxides and α-Al_2O_3 will nucleate and grow. However, if the oxygen partial pressure is too low, then spinel oxides will not form, and only α-Al_2O_3 will be present. This is what is thought to have occurred during the heat treatment. Although the heat treatment is nominally carried out in vacuum, there is still some oxygen present. Assuming sufficient oxygen was present to form a thin α-Al_2O_3 layer, the presence of this α-Al_2O_3 layer will act as a barrier which separates the coating from the environment during the subsequent oxidation experiments. Hence, nucleation of spinel oxides is prevented and the α-Al_2O_3 grows slowly. For the as-sprayed coatings there is no such pre-existing α-Al_2O_3 layer, and hence, spinels and α-Al_2O_3 both form.

It should be noted that this study is part of a larger, on-going comparative study of HVOF and VPS CoNiCrAlY coatings. Here, one HVOF coating has been compared with one VPS coating, neither of which has necessarily been produced using optimal spraying conditions. A thorough study will have to include several sprayings of HVOF and VPS coatings using different process parameters. Comparison between the full set of coatings will enable behavior linked to spraying type to be distinguished from behavior due to variations in the process parameters within each process.

4. Conclusions

Because of the different temperature exposures of the feedstock powder during HVOF and VPS spraying, the

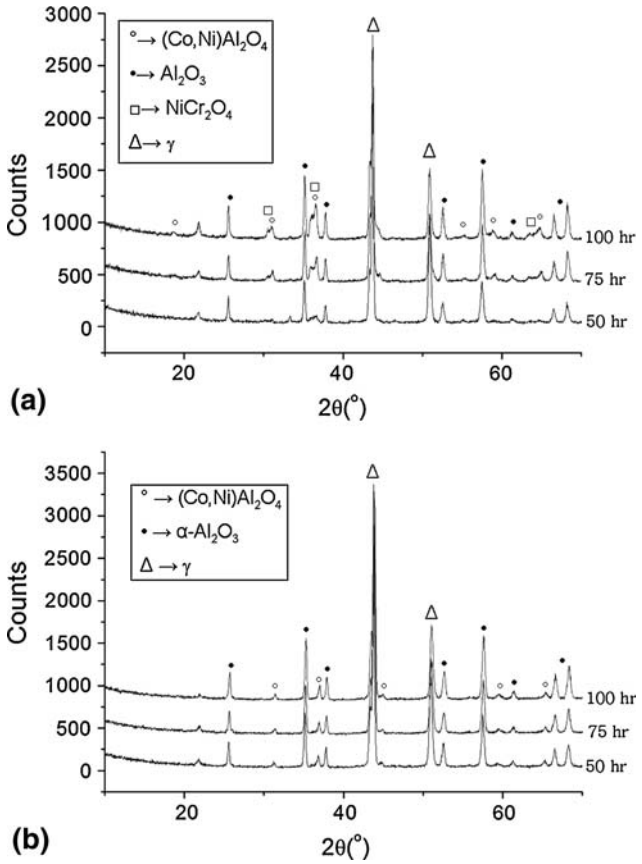

Fig. 9 XRD patterns from the heat-treated oxidized surfaces for different oxidation times, (a) VPS, (b) HVOF

as-sprayed HVOF coating retains the γ/β microstructure of the feedstock powder whereas the VPS coating generally consists of a single (γ) phase. In both cases, free-standing coatings were successfully produced.

A 3-h, 1100 °C heat treatment converts the single (γ) phase of the as-sprayed VPS coating to a two-phase γ/β microstructure. The same heat treatment coarsens the γ/β microstructure of the as-sprayed HVOF coating.

Prior heat treatment increases the parabolic rate constant, K_p, for both types of coatings. This is attributed to a sintering effect eliminating porosity from the coating during heat treatment.

Both as-sprayed and heat-treated HVOF coatings have lower K_p values than the corresponding VPS coatings. This is explained as being due to the presence of oxides in the HVOF coatings, which act as barrier to diffusion. Such oxides are apparently absent from the VPS coatings.

Oxidation of the free-standing as-sprayed coatings produces a dual-layer oxide consisting of an inner layer of α-Al_2O_3 and an outer spinel layer. Oxidation of heat-treated samples results in the formation of a single layer, α-Al_2O_3, oxide. This is attributed to the formation of a thin α-Al_2O_3 layer during heat treatment which prevents nucleation and growth of spinel oxides during the subsequent oxidation exposure.

Acknowledgments

We acknowledge with thanks the facilities that were provided to make the VPS coatings at The University of Cambridge, courtesy of Prof. T.W. Clyne and with the assistance of Mr K.A. Roberts.

References

1. J. Toscano, R. Vaben, A. Gil, M. Subanovic, D. Naumenko, L. Singheiser, and W.J. Quadakkers, Parameters Affecting TGO Growth and Adherence on MCrAlY-bond Coats for TBC's, *Surf. Coat. Technol.*, 2006, **201**, p 3906-3910 (in English)
2. W. Brandl, G. Marginean, D. Maghet, and D. Utu, Effects of Specimen Treatment and Surface Preparation on the Isothermal Oxidation Behavior of the HVOF-sprayed MCrAlY Coatings, *Surf. Coat. Technol.*, 2004, **188-189**, p 20-26 (in English)
3. W. Brandl, H.J. Grabke, D. Toma, and J. Krüger, The Oxidation Behaviour of Sprayed MCrAlY Coatings, *Surf. Coat. Technol.*, 1996, **86-87**, p 41-47 (in English)
4. M.P. Taylor, An Oxidation Study of an MCrAlY Overlay Coating, *Mater. High Temp.*, 2005, **22**, p 433-436 (in English)
5. D. Zhang, S.J. Harris, and D.G. McCartney, Mechanical Properties and Microstructure of HVOF Sprayed Co and Ni Alloy Coatings, Thermal Spray 2003, *Proceedings of the International Thermal Spray Conference*, (Orlando, FL, USA), ASM International, 2003, p 829-836 (in English)
6. R. Prescott and M.J. Graham, The Formation of Aluminium Oxide Scales on High-temperature Alloys, *Oxid. Met.*, 1992, **38**, p 233-254 (in English)
7. F. Tang, L. Ajdelsztajn, and J.M. Schoenung, Effects of Cryomilling on the Oxidation of Thermally Sprayed MCrAlY, Thermal Spray 2004, *Proceedings of the International Thermal Spray Conference*, (Osa Japan), 2004, p 148-153 (in English)
8. F. Tang, L. Ajdelsztajn, G.E. Kim, V. Provenzano, and J.M. Schoenung, Effects of Surface Oxidation During HVOF Processing on the Primary Stage Oxidation of a CoNiCrAlY Coating, *Surf. Coat. Technol.*, 2004, **185**, p 228-233 (in English)
9. H. Choi, B. Yoon, H. Kim, and C. Lee, Isothermal Oxidation of Air Plasma Spray NiCrAlY Bond Coatings, *Surf. Coat. Technol.*, 2002, **150**, p 297-308 (in English)
10. P. Poza and P.S. Grant, Microstructure Evolution of Vacuum Plasma Sprayed CoNiCrAlY Coatings After Heat Treatment and Isothermal Oxidation, *Surf. Coat. Technol.*, 2006, **201**, p 2887-2896 (in English)
11. K. Fritscher and Y.T. Lee, Investigation of an As-Sprayed NiCoCrAlY overlay Coating—Microstructure and Evolution of the Coating, *Mater. Corros.*, 2005, **56**(1), p 5-14 (in English)
12. L. Ajdelsztajn, J.A. Picas, G.E. Kim, F.L. Bastian, J. Schoenung, and V. Provenzano, Oxidation Behavior of HVOF Sprayed Nanocrystalline NiCrAlY Powder, *Mater. Sci. Eng. A*, 2002, **338**, p 33-43 (in English)
13. V. Higuera, F.J. Belzunce, and J. Riba, Influence of the Thermal-spray Procedure on the Properties of a CoNiCrAlY Coating, *Surf. Coat. Technol.*, 2006, **200**, p 5550-5556 (in English)
14. R. Mobarra, A.H. Jafari, and M. Karaminezhaad, Hot Corrosion Behavior of MCrAlY Coatings on IN738LC, *Surf. Coat. Technol.*, 2006, **201**(6), p 2202-2207
15. M. Shibata, S. Kuroda, M. Watanabe, and Y. Sakamoto, Oxidation Property of CoNiCrAlY Coatings Prepared by Various Thermal Spraying Techniques, *Materials Science Forum*, 2006, **522-523**, p 339-344
16. A. Feuerstein, J. Knapp, T. Taylor, A. Ashary, A. Bolcavage, and N. Hitchman, Technical and Economical Aspects of Current Thermal Barrier Coating Systems for Gas Turbine Engines by Thermal Spray and EBPVD: A Review, *J. Therm. Spray Tech.*, 2008, **17**(2), p 199-213
17. Y. Itoh, M. Saitoh, and M. Tamura, Characteristics of MCrAlY Coatings Sprayed by High Velocity Oxy-fuel Spraying System, *J. Eng. Gas Turb. Power*, 2000, **122**, p 43-49

18. W. Brandl, D. Toma, J. Krüger, H.J. Grabke, and G. Matthäus, The Oxidation Behaviour of HVOF Thermal-sprayed MCrAlY Coatings, *Surf. Coat. Technol.*, 1997, **94-95**, p 21-26 (in English)
19. C.H. Lee, H.K. Kim, H.S. Choi, and H.S. Ahn, Phase Transformation and Bond Coat Oxidation Behavior of Plasma-sprayed Zirconia Thermal Barrier Coating, *Surf. Coat. Technol.*, 2000, **124**, p 1-12 (in English)
20. F. Tang, L. Ajdelsztajn, and J.M. Schoenung, Characterisation of Oxide Scales Formed on HVOF NiCrAlY Coatings with Various Oxygen Contents Introduced During Thermal Spraying, *Scripta Mater.*, 2004, **51**, p 25-29 (in English)